*metals*

MDPI

*Article*

# Grain Growth during Mechanical Processing of Austenitic Stainless Steel AISI 321

**Liudmila V. Radionova [1,*], Danil V. Perevozchikov [2], Aleksandr N. Makoveckii [2], Victor N. Eremin [2], Alexander M. Akhmedyanov [3] and Sergey V. Rushchits [3]**

[1] Department of Metallurgy, Moscow Polytechnic University, Bolshaya Semyonovskaya Str. 38, Moscow 107023, Russia
[2] PJSC "ChelPipe", Mashinostroiteley Str. 21, Chelyabinsk 454129, Russia; danil.perevozchikov@chelpipegroup.com (D.V.P.); aleksandr.makoveckiy@chelpipegroup.com (A.N.M.); veremin@chelpipegroup.com (V.N.E.)
[3] Department of Material Science and Physics and Chemistry of Materials, South Ural State University, Lenin Prospect 76, Chelyabinsk 454080, Russia; akhmedianovam@susu.ru (A.M.A.); rushchitcsv@susu.ru (S.V.R.)
* Correspondence: radionovalv@rambler.ru; Tel.: +7-951-231-9332

**Abstract:** The kinetics of austenite grain growth during thermomechanical treatment of AISI 321 steel with a relatively high content of carbon (0.07 wt. %) and titanium (0.50 wt. %) were studied. Hot deformation was carried out by the uniaxial compression of cylindrical specimens on a Gleeble 3800 thermomechanical simulator. A dependence is obtained for calculating the kinetics of austenite grain growth for a temperature range of 1150–1250 °C. The proposed dependence makes it possible to evaluate grain growth under non-isothermal conditions. The verification of the adequacy of the proposed dependence and the method for calculating the grain size at cooling rates 0.2, 1 and 5 °C/s showed its high convergence. The difference between the calculated and experimental grain size did not exceed 8%. The suppression of grain growth is due to the precipitation of titanium carbides and carbonitrides. Using the developed grain growth model, an analysis was made of the reasons for the formation of large grains in the shell after the elongating in the production process.

**Keywords:** pipe rolling; hot deformation; grain growth kinetics; austenitic stainless steel; AISI 321



**Citation:** Radionova, L.V.; Perevozchikov, D.V.; Makoveckii, A.N.; Eremin, V.N.; Akhmedyanov, A.M.; Rushchits, S.V. Grain Growth during Mechanical Processing of Austenitic Stainless Steel AISI 321. *Metals* **2023**, *13*, 1421. https://doi.org/10.3390/met13081421

Academic Editors: Angelo Fernando Padilha and C. Issac Garcia

Received: 4 June 2023
Revised: 4 August 2023
Accepted: 7 August 2023
Published: 8 August 2023



## 1. Introduction

Stainless steel is used in industries such as construction [1], medicine [2], energy [3], food [4] and chemical [5,6]. Austenitic stainless steel pipes are used in the nuclear power industry [7–9]. Nuclear power pipes are subjected to cyclic mechanical loadings caused by internal pressure fluctuations, coupled with strain cycles due to start up/shut down or thermal transients [10]. Accordingly, thermomechanical fatigue failure has become one of the main limited factors for the service life of nuclear power pipelines [7]. In addition, during long-term servicing conditions under elevated temperatures and pressures, mechanical loads and dead weight lead to the accumulation of creep damage [7]. In all these industries, materials are subject to requirements for tensile strength and yield strength, corrosion resistance and other properties. These properties of metal products are affected by the grain size.

Austenitic stainless steel is generally 100% austenite ($\gamma$) or austenite with a small amount of $\delta$-ferrite [11]. The presence of $\delta$-ferrite particles reduces the corrosion resistance of austenitic steels, especially their resistance to intergranular corrosion (IGC), and affects the susceptibility of austenitic steels to stress corrosion cracking, fatigue strength and creep resistance nonuniformly [12].

The grain size of austenite after hot deformation depends on dynamic recrystallization and subsequent grain growth. Here are just some of the studies [13–16] on the effect of grain

size on the properties of austenitic steels. Issues related to the dynamic recrystallization of austenitic stainless steel are discussed in detail in this study [17].

One of the processes that affect the formation of the final grain size is grain growth after recrystallization [18,19]. The grain size formed during recrystallization depends mainly on the plastic deformation degree, the temperature at which recrystallization occurs and the holding time of the steel. Alloying elements dissolved in austenite hinder grain growth and reduce grain boundary mobility. To an even greater extent, grain growth is inhibited by the dispersed precipitates of secondary phases. The strongest influence on the tendency to austenite grain growth is exerted by the addition of carbide-forming or nitride-forming elements (V, Nb, Ti, Al), if these elements precipitate in the form of the corresponding carbides (NbC, TiC), nitrides (VN, AlN, NbN, TiN) or carbonitrides. In such steels, the growth of austenite grains is significantly inhibited up to the temperature at which the dissolution of the above precipitates in austenite begins. The dissolution of small particles along the boundaries of some grains leads to the intensive growth of these selected grains, called abnormal growth or secondary recrystallization. As a result of anomalous growth, a structure that is extremely heterogeneous in grain size is formed. On the contrary, relatively uniform grain growth at temperatures below the beginning of the dissolution of particles and above the temperature of their complete dissolution, leading to the formation of a homogeneous grain structure, is usually called normal growth. For designing technological modes of material processing, it is useful to have a mathematical model that describes the kinetics of the grain growth process.

Many researchers in the middle of the 20th century theoretically derived a parabolic law [20–22], which describes the kinetics of grain growth,

$$D^2 - D_0^2 = K \cdot t \tag{1}$$

where $D_0$—initial grain size, μm; $D$—grain size (μm) at the time $t$, (s); $K$—function depending on the holding temperature $T$ and the activation energy of grain growth $Q$, (KJ/mol),

$$K = A \cdot \exp\left(-\frac{Q}{RT}\right) \tag{2}$$

where $A$—the material constant, $\mu m^{1/m} \cdot s^{-1}$; $R$ = 8.314 J/(K·mol)—universal gas constant.

When constructing empirical models of grain growth kinetics, it usually turned out [17–19] that the dependence of grain growth has a power law form,

$$D^m - D_0^m = K \cdot t \tag{3}$$

where $m \neq 2$—material constant.

Dependences of this type were obtained when studying the kinetics of grain growth in austenitic stainless steels [23,24], low alloy steels [25,26] and other metals and alloys [27–31].

Note that most often, researchers limit themselves to studying the kinetics of grain growth only under isothermal conditions. In the framework of some works, experiments were carried out to study grain growth under non-isothermal conditions [32–34]. However, studies on the non-isothermal process of grain growth in Cr-Ni austenitic stainless steel are not found in scientific articles.

Perhaps this is due to the fact that to create controlled non-isothermal conditions with given heating or cooling rates, specialized equipment is required which is not always available to researchers. At the same time, in many real production processes, the temperature of the material changes. For example, if the welding process is considered, regardless of the type of heat source, there is a thermal influence zone within which the temperature field is non-isothermal throughout the entire welding cycle.

Non-isothermal periods of the process can be neglected only in cases where their duration is short compared to the duration of the isothermal period. This occurs during annealing (especially during rapid heating and cooling).

Another example of grain growth under non-isothermal conditions is grain growth in shells after they have been pierced. This is what prompted this study. It should be understood the reasons for the formation of a coarse-grained structure in the production of pipes at the Chelyabinsk Pipe Rolling Plant. The technological scheme (Figure 1) for the production of pipes includes the following operations and features:

1. A billet machined and drilled with an outer diameter of ~600 mm and an internal through axial hole of ~100 mm;
2. Heating the billet to a temperature of ~1280 °C;
3. Firmware on the cross-helical rolling mill;
4. Cooling the metal to room temperature;
5. Heating the shell to a temperature of ~1280 °C;
6. Elongating on a helical rolling mill, after which a shell with an outer diameter of ~650 mm and a wall thickness of ~70 mm is obtained;
7. Machining to the size of the finished pipe 63 × 10 mm$^2$.

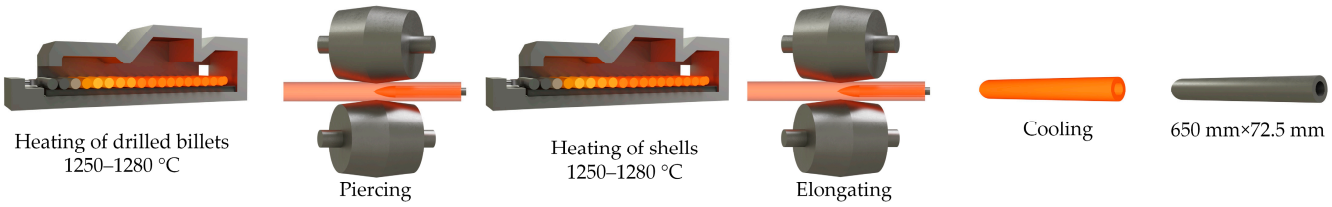


**Figure 1.** Technological scheme for the production of pipes 630 mm × 10 mm.

In the microstructure of steel pipes after piercing, an equiaxed grain is observed throughout the entire wall thickness. In this case, the grain size along the wall thickness is different. The grain size increases from the outer to the inner surface of the pipe wall (Figure 2). When machining pipes up to a wall thickness of 10 mm, metal layers with a large grain size are removed. However, the presence of coarse-grain in the pipe wall limits the range of pipes produced by the Chelyabinsk Pipe Rolling Plant and reduces the profitability of the plant.

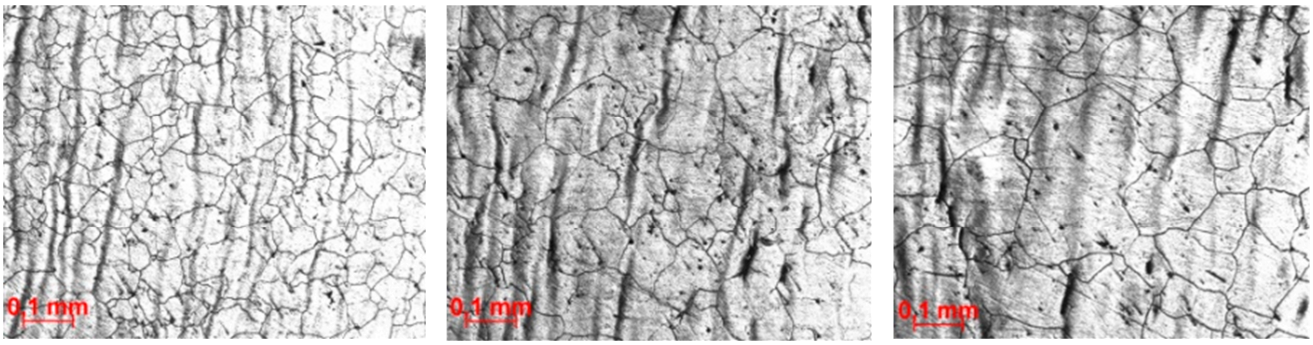


(**a**) (**b**) (**c**)

**Figure 2.** The microstructure of the steel shell at different distances from the outer surface: (**a**)—10 mm; (**b**)—25 mm; (**c**)—50 mm.

The purpose of this work is to study the grain growth kinetics in austenitic stainless steel and to identify the reasons for the formation of large grains during the production of hot-rolled pipes from this steel.

## 2. Materials and Methods

The chemical composition of the austenitic stainless steel used in the present study is shown in Table 1.

**Table 1.** Chemical composition (wt %) of the AISI 321 steel.

| C | Si | Mn | Cr | Ni | S | P | Mo | Cu | Ti | N |
|---|---|---|---|---|---|---|---|---|---|---|
| 0.07 | 0.30 | 1.33 | 17.7 | 10.3 | 0.005 | 0.025 | 0.19 | 0.19 | 0.50 | 0.014 |

The samples in the form of cylinders with 15 mm length and 10 mm diameter were cut out of the tube after the piercing, in the radial direction. Hot deformation was carried out by uniaxial compression test on a simulator of thermomechanical processes, Gleeble 3800. The temperature of the sample during the test was measured by a thermocouple welded to its central part. Before deformation, the samples were heated to a temperature of 1280 °C and held for 10 min. 1280 °C is a typical temperature for heating cast blanks before subsequent hot deformation. Then, the samples were cooled to a temperature of 1200 °C and deformed at this temperature with a strain rate of $\dot{\varepsilon} = 1\ s^{-1}$ and up to a true strain of $\varepsilon = 0.7$. This mode of preliminary hot deformation was accompanied by dynamic recrystallization and ensured the formation of recrystallized grains with an average size of $D_0 = 40$ μm.

The first series includes isothermal tests. The samples were held at the same temperature of 1200 °C for 1, 5 or 15 min. The next samples for a short time were cooled (or heated) to a holding temperature of 1100, 1150 or 1250 °C (Figure 3) and held also for 1, 5 or 15 min (Table 2). After holding, every sample was quenched with a jet of water.

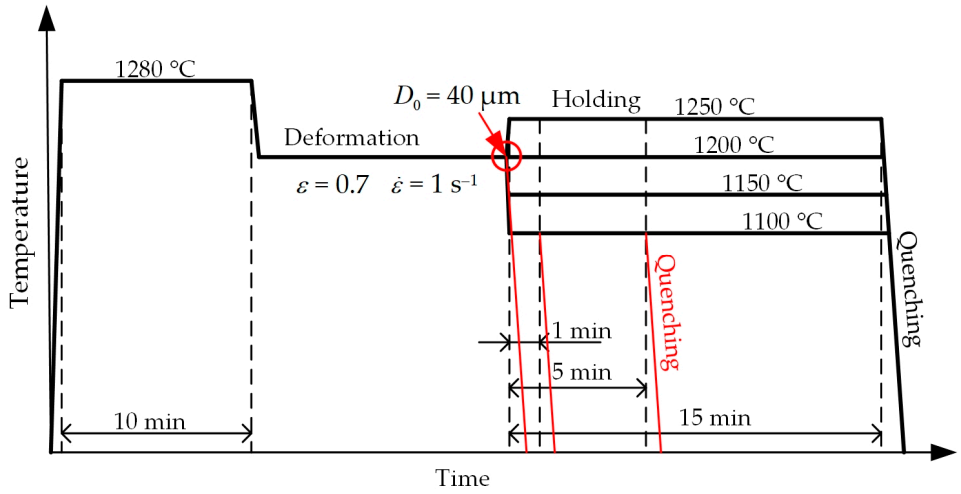


**Figure 3.** Schematic of the experiment at isothermal mode.

**Table 2.** Modes for studying the kinetics of grain growth at isothermal mode.

| **Holding Temperature, °C** | **1100** | | | **1150** | | | **1200** | | | **1250** | | |
|---|---|---|---|---|---|---|---|---|---|---|---|---|
| Holding time, min | 1 | 5 | 15 | 1 | 5 | 15 | 1 | 5 | 15 | 1 | 5 | 15 |
| Average size grains, μm | 43 | 44 | 45 | 76 | 100 | 125 | 90 | 120 | 160 | 110 | 150 | 196 |

The secondary series includes non-isothermal tests. The samples were cooled at a controlled constant rate. The cooling rate was controlled by passing an electric current through the samples. The cooling rate was 0.2, 1 and 5 °C/s. The schematic of the experiment is shown in Figure 4. For each mode, 3 samples were processed.

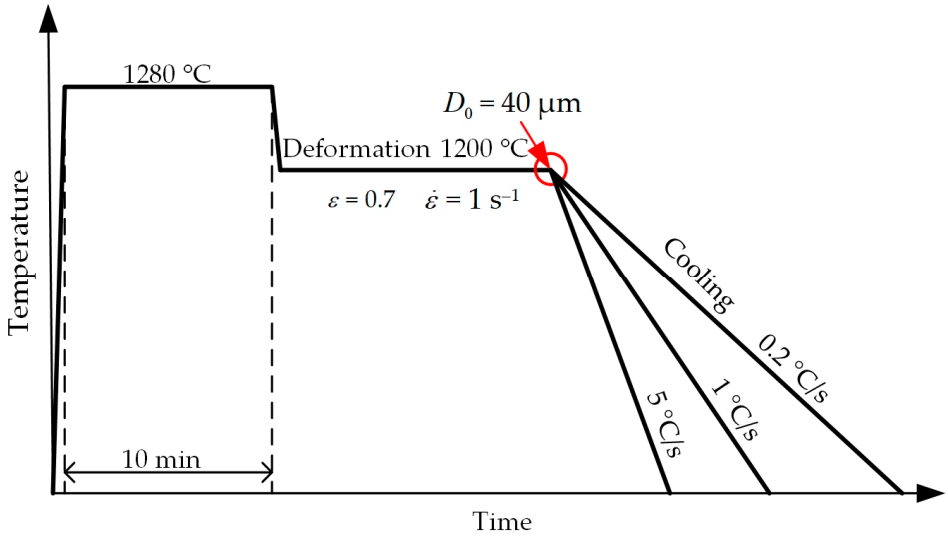


**Figure 4.** Schematic of the experiment at non-isothermal temperatures.

Microstructural studies were performed using an optical microscope C. Zeiss Observer (Carl Zeiss AG, Oberkochen, Germany). The slots made from the longitudinal section of the samples were subjected to electrolytic etching in a 4% solution of nitric acid in ethanol. The grain size was determined by the intersection method.

## 3. Results and Discussion

The microstructures obtained during studies in isothermal conditions (Figure 3) are shown in Figure 5. The microstructure of the studied steel AISI 321 consists of austenite (ɣ) grains and contains a small amount of δ-ferrite. The microstructure of the sample after primary deformation at a temperature of 1200 °C with a deformation rate of 1 $s^{-1}$ is shown in Figure 5a. The microstructures obtained during experimental deformation and subsequent holding at temperatures of 1250, 1150 and 1100 °C for 15 min are shown in Figure 5b–d, respectively. Holding at a temperature of 1100 °C is accompanied by a slight growth of grains, while areas are preserved in which the grain size practically does not change. As a result, a structure with a heterogeneous granular structure is formed.

With an increase in the holding temperature to 1150 and 1250 °C, the intensive growth of austenite grains begins. The emerging structure becomes coarse-grained and homogeneous.

According to the results of measuring the grain size for all processing modes of the studied samples (Figure 3 and Table 2), the dependences of the average grain size on the exposure time were plotted (Figure 6).

Figure 6 shows experimental data on grain size depending on temperature and holding time. From the data in Figure 6, it can be concluded that grain growth at a temperature of 1100 °C compared to higher temperatures is largely suppressed, probably by particles of carbides or carbonitrides of titanium released at this temperature [35,36]. It is worth noting that in the steel of the considered chemical composition, the suppression of other recrystallization processes was previously noted [37,38], which confirms the version of the precipitation of carbides.

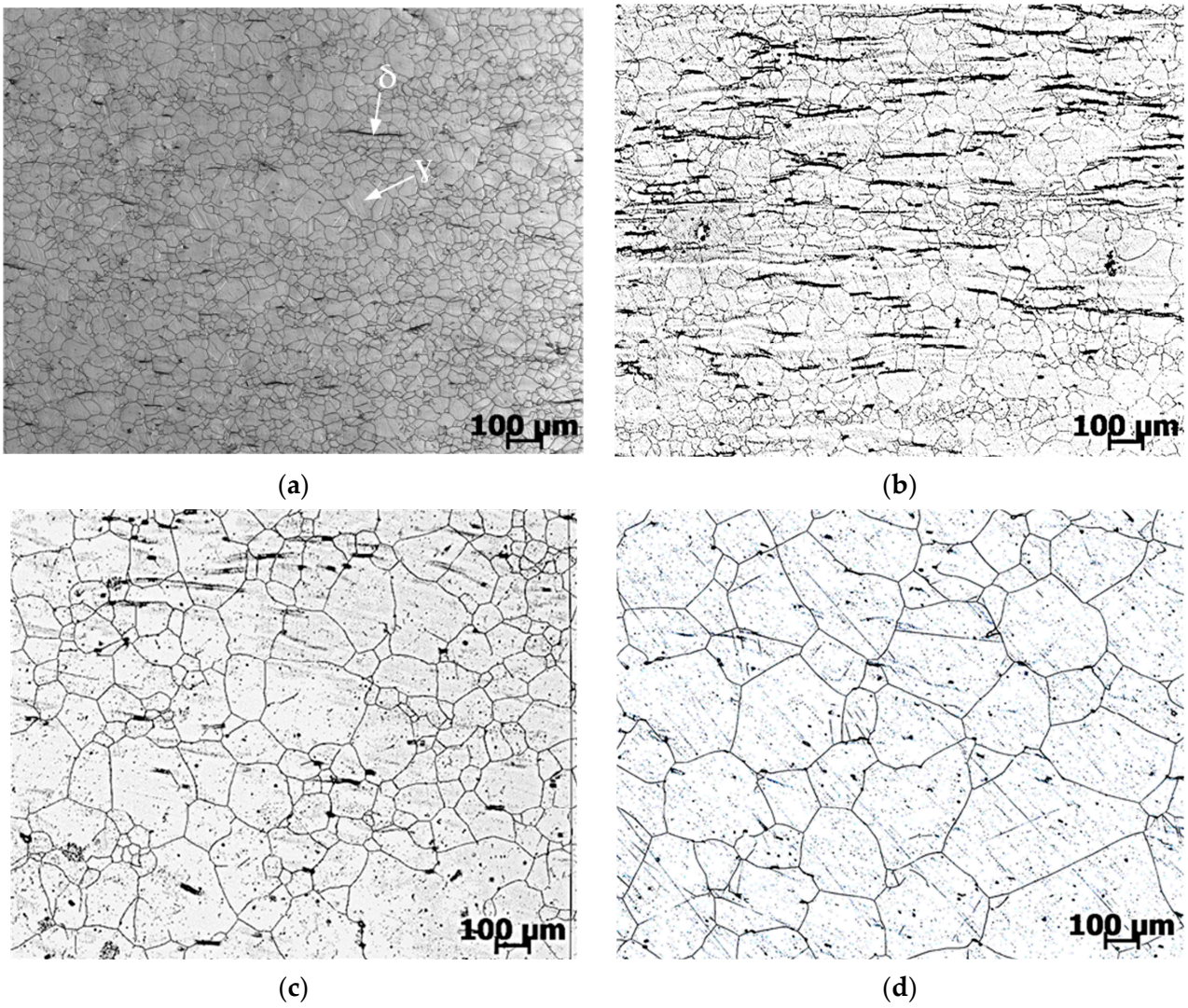


**Figure 5.** Microstructure of AISI 321 steel after recrystallization: (**a**) quenching after deformation at 1200 °C; (**b**) holding at 1100 °C, 15 min; (**c**) holding at 1150 °C, 15 min; (**d**) holding at 1250 °C, 15 min.

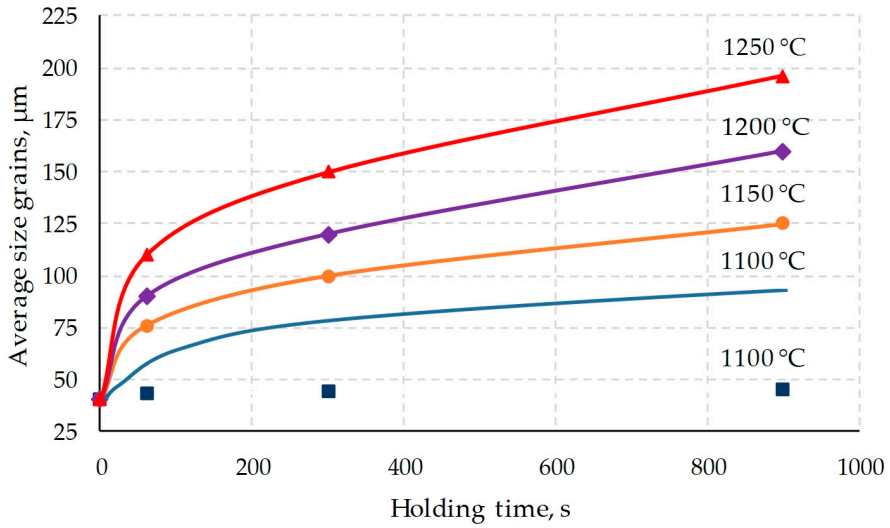


**Figure 6.** Growth kinetics of recrystallized austenite grains of AISI 321 steel: points—experimental data; solid lines—calculation by Equation (3).

In the work [39], it was also found that the amount of titanium significantly affects the recrystallization of steel during hot deformation. The studies were carried out on AISI 321 steel with a Ti = 0.50% content (Table 1) and with a reduced Ti = 0.21%. Studies have shown that in the temperature range of 1280–1100 °C, in steel with both increased (0.50%) and reduced (0.21%) titanium content, dynamic recrystallization proceeds in full at a strain rate of 0.01, 0.1, 1 $s^{-1}$. When the temperature drops below 1100 °C, there is a difference in the behavior of steel during hot deformation. In steel with a titanium content of 0.50%, deformation at a temperature of 1100 °C at a rate of 0.1 $s^{-1}$ causes only partial dynamic recrystallization, while in steel with a reduced titanium content (0.21%) it passes completely. Thus, dynamic recrystallization in steel with a low titanium content in the temperature range of 1100 °C proceeds to a greater extent than in steel with a high content of these elements.

The results obtained by us in the work [39] indirectly also confirm the assumption that the reason for the delay in dynamic recrystallization and grain growth in steel with the chemical composition indicated in Table 1, below a temperature of 1100 °C, are inclusions of titanium carbides.

As mentioned earlier, the kinetics of grain growth are usually described using Equations (2) and (3).

Using the method of regression analysis, the coefficients $m$, $A$ and $Q$ were found from expressions (2) and (3) describing the kinetics of grain growth:

$m = 4.752$;

$A = 1.669 \times 10^{20} \mu m^{1/m}\ s^{-1}$;

$Q = 359.4$ KJ/mol.

The formula for determining the grain size of austenite under non-isothermal conditions will be as follows:

$$D^{4.752} - D_0^{4.752} = 1.669 \times 10^{20} \cdot \exp\left(-\frac{359400}{8.314 \cdot T}\right) \cdot t. \quad (4)$$

To determine the coefficients, only data obtained at holding temperatures of 1150, 1200 and 1250 °C were used. The values obtained at 1100 °C were excluded from consideration since at this temperature the behavior of steel differs from the general pattern.

According to Formula (4), the grain growth curves were calculated at holding temperatures of 1100, 1150, 1200 and 1250 °C, which are presented in the form of solid lines in Figure 6. The curve for a temperature of 1100 °C lies much higher than corresponding experimental points, which once again indicates the suppression of grain growth at a temperature of 1100 °C.

Taking into account the results presented in Figure 6, it follows that the obtained Formula (4) cannot be used to predict the grain size when it grows below a temperature of 1100 °C. The results obtained will be erroneous.

The microstructure of the samples obtained by deformation and subsequent cooling at a controlled rate is shown in Figure 7. Steel exhibits an austenitic structure with a small fraction of δ-ferrite. From photographs of microstructures, it can be seen that a decrease in the cooling rate leads to an increase in grain size. Thus, a decrease in the cooling rate to 0.2 °C/s leads to an increase in the average grain size from 40 μm (after quenching) to 108 μm. Grain sizes determined by the intersection method are presented in Table 3.

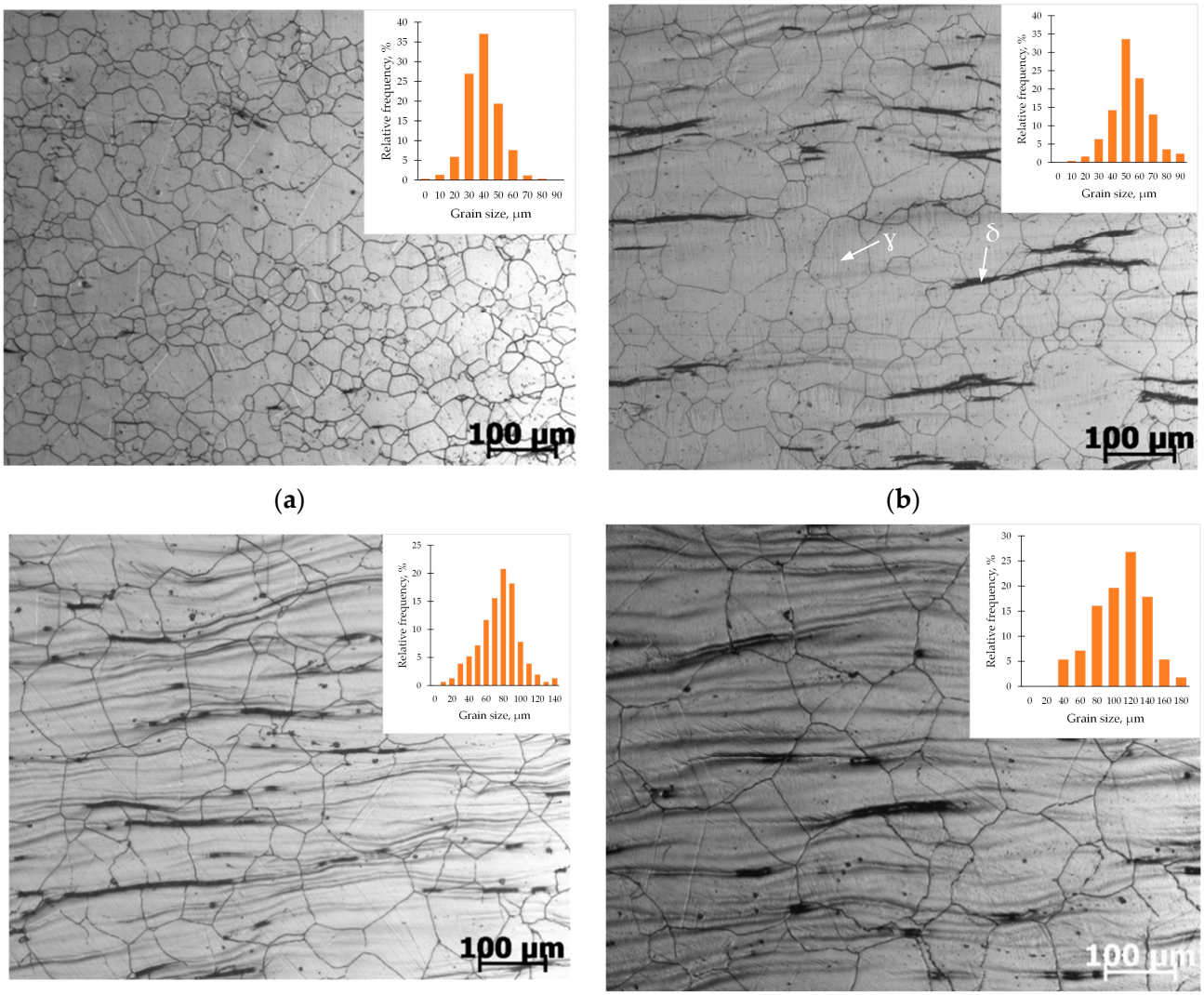


**Figure 7.** AISI 321 steel microstructure after cooling at a rate of: (**a**) Quenching (immediately cooling); (**b**) 5 °C/s; (**c**) 1 °C/s; (**d**) 0.2 °C/s.

**Table 3.** Experimental and calculated austenite grain size.

| Cooling Rate, °C/s | Experimental Grain Size (Average), μm | Calculated Grain Size, μm | Difference between Calculated and Experimental Value, % |
|---|---|---|---|
| Quenching (immediately cooling) | 40 | - | - |
| 5 | 55 | 60 | 8 |
| 1 | 75 | 82 | 8 |
| 0.2 | 108 | 114 | 5 |

Empirical expression (4), describing the growth of austenite grains under isothermal conditions, can be used to predict grain growth under non-isothermal conditions. To do this, the time interval for cooling is divided into small intervals, the temperature difference in which has a relatively low value (within 1 °C). Further, the process of grain growth over a small interval is considered as for an isothermal process.

The calculated values of the grain size of austenite obtained by this method are shown in Table 3. The difference in the calculated and experimental values of the austenite grain

size does not exceed 8%, which is acceptable for predicting the microstructure under production conditions. It follows that the method used to calculate the grain size formed in a non-stationary temperature field is applicable to solving practical problems arising in production processes.

Using Equation (4) obtained in the course of laboratory experiments, the reasons for the formation of a coarse-grained structure in the shell were analyzed in the production of pipes using the above technology (Figure 1).

To calculate according to Equation (4), it is necessary to determine the temperature distribution over the billet metal using the heat conduction equation. To simplify the task, the following assumptions were made:

- The metal is cooled equally in all directions, i.e., the problem is axisymmetric;
- Heat transfer through the ends of the shell is neglected, so the solution can be considered valid for points remote from the end of the shell.

Taking into account the assumptions made, it is obtained the heat conduction equation in the polar coordinate system [40] is:

$$\rho c \frac{\partial T}{\partial t} = \frac{\lambda}{r} \frac{\partial}{\partial r} \left( r \frac{\partial T}{\partial r} \right) \quad (5)$$

where $\rho$—the density of the material, kg/m$^3$; $T$—the billet temperature, K; $C$—the heat capacity of the material J/(kg·K); $\lambda$—thermal conductivity of the material W/(kg·K); $t$—time, s; $r$—coordinate characterizing the distance of the point from the axis of the billet, m.

To solve the heat conduction equation, it was assumed that the density of steel does not depend on temperature and is equal to 7900 kg/m$^3$. The heat capacity and thermal conductivity coefficients were calculated using the JMatPro program [41].

The initial conditions for the temperature distribution (Figure 8) were determined earlier by the finite element method when modeling the piercing of the billet.

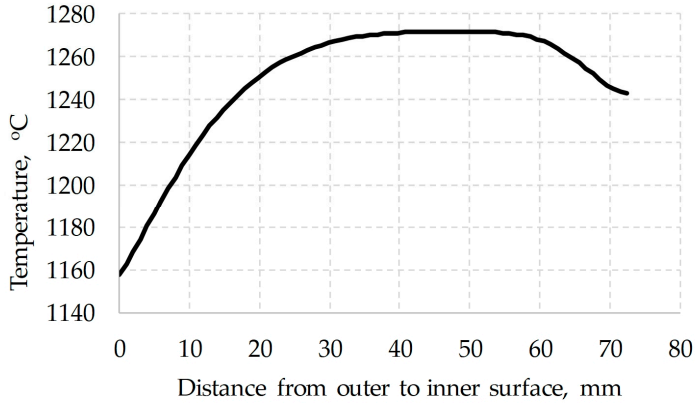


**Figure 8.** Temperatures over the section of the billet.

Usually, heat exchange between a solid and a gas occurs in two ways [42,43]:

- Convection for which the heat flow is calculated according to the Newton-Richmann law;
- Radiation for which the heat flux is calculated according to the Stefan–Boltzmann law.

Based on this, boundary conditions were formulated: in the form of Equations (6) for the inner surface and (7) for the outer surface.

$$r = \frac{d_{\text{int}}}{2} : \frac{\partial T}{\partial r} = \alpha (T_{\text{int}} - T_{air}), \; t \geq 0 \quad (6)$$

where $r$—coordinate characterizing the distance of the point from the axis of the billet, m; $T$—the billet temperature, K; $d_{\text{int}}$—inner diameter, mm; $T_{\text{int}}$—the temperature of the inner

surface of the metal, K; $T_{air}$—the air temperature inside the hole, K; α—the convection heat transfer coefficient.

$$r = \frac{D}{2} : \lambda \frac{\partial T}{\partial r} = \alpha(T_{env} - T_{out}) + \sigma\varepsilon\left(T_{env}^4 - T_{out}^4\right),\ t \geq 0 \quad (7)$$

where $T_{env}$—the ambient temperature, K; $T_{out}$—temperature of the outer surface, K; $\sigma$—Stefan-Boltzmann constant; $\varepsilon$—emissivity factor.

Note that Equation (6) does not include a component describing the heat flux by radiation, since the inner surface radiates heat to itself. Cooling occurs only by convection, and air flows around the inner surface of the shell wall.

The heat conduction equation was solved by the finite difference method, using Samarskii's implicit four-point difference scheme [44,45]. When using the Samarsky scheme, the calculation of temperature at each time step is reduced to solving a system of algebraic equations using sweep coefficients. In the process of solving, the wall of the shell was divided into $N$ segments of length $\Delta r$. The metal temperature at each time step $\Delta t$ was calculated at each point $r_i$. The coordinate of the points is calculated by the formula:

$$r_i = \frac{d_{\text{int}}}{2} + \Delta r \cdot (i - 1) \quad (8)$$

where $i$—index, integers from 1 to n.

The cooling rate calculated by this method is shown in Figure 9.

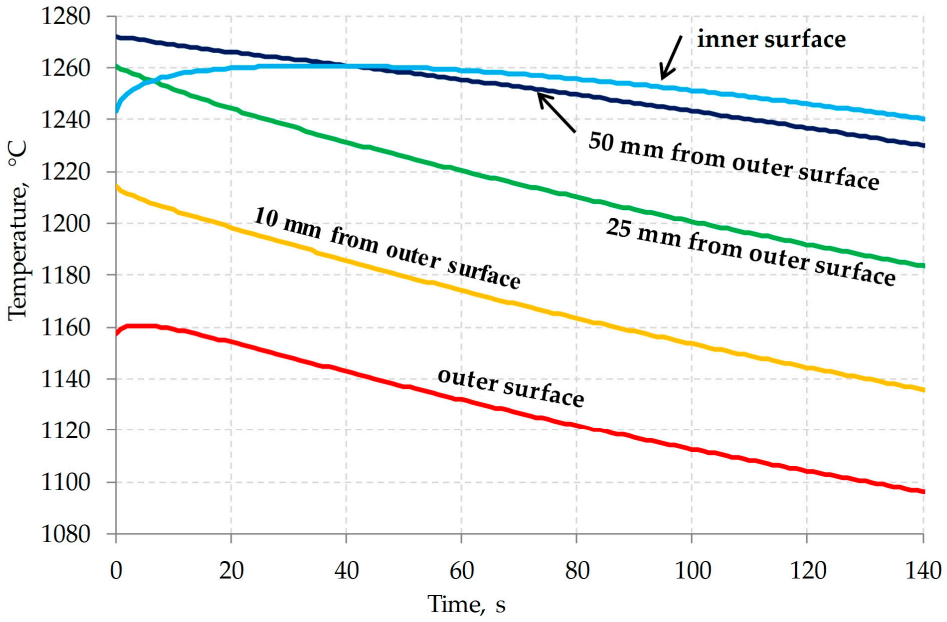


**Figure 9.** Cooling kinetics of the shell cross-section after issuance from the piercing mill.

As can be seen in Figure 9, the temperature of the inner surface of the shell rises in the first 20 s. This is due to the fact that after removing the cold piercing plug from the shell, the inner surface heats up due to heat transfer in the wall.

Simultaneously with the calculation of thermal conductivity, the kinetics of grain growth were calculated. Actions are performed in the following sequence:

1. The temperature distribution was calculated at a time step at each $i$-th point.
2. The value of the grain size $D$ at the end of the time step was calculated by Formula (4) separately for each point. The just calculated value at the point was substituted as the temperature value.
3. A transition to a new step is performed. In the next step, the obtained value of the grain size at this point is used as the initial grain size $D_0$ in Formula (4).

To calculate such a sequence, it is necessary to determine the grain size at the initial moment of time. In the works [17,44,45] previously published by our team of authors, the process of dynamic recrystallization in steel of the current chemical composition was considered. The activation energy dynamic recrystallization, the equation for calculating the Zener–Holomon parameter, the strain required to complete the first cycle of dynamic recrystallization, the grain size formed during dynamic recrystallization, and other parameters were determined. Figure 10 shows a map of grain sizes depending on the strain rate and temperature. In the form of dotted lines, the ranges of deformation speed and temperature inherent in different layers of the shell have been marked. As can be seen in Figure 10, at the end of the piercing process, grains ranging in size from 20 to almost 80 μm can be formed. Note that the temperature of the metal in the middle of the shell wall at this moment is about 1260 °C. As you can see in Figure 11, the initial grain with a size of 0 and 70 μm, after 6–7 s, differs in size by no more than 10 μm. For this reason, without any large error in estimating the final grain size, it can be assumed that the initial grain at the initial time is 25 μm. Taking into account this condition ($D_0$ = 25 μm), the kinetics of grain growth were calculated. The calculation results are shown in Figure 12.

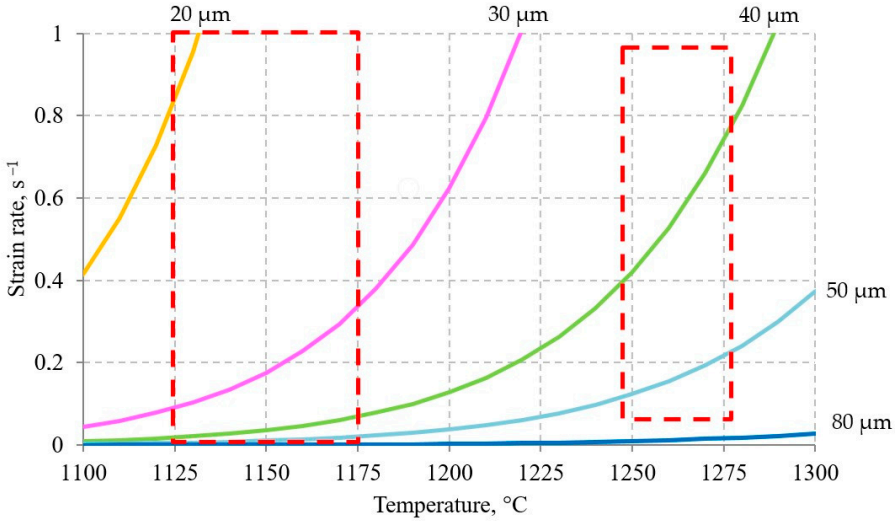


**Figure 10.** Map of dynamically recrystallized grains during piercing shell.

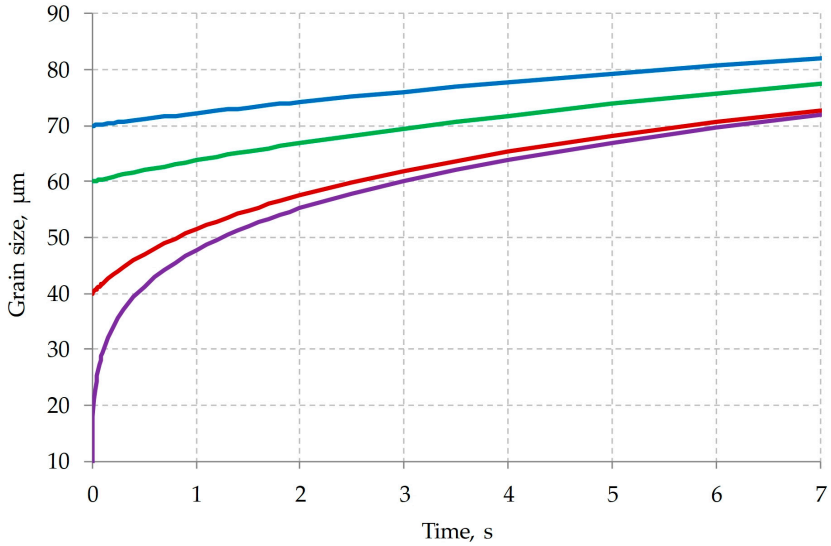


**Figure 11.** Dependence of the grain size on time, in the case of metal cooling at a uniform rate of 1 °C/s from the initial temperature of 1260 °C ($D_0$: 3, 40, 60 and 70 μm).

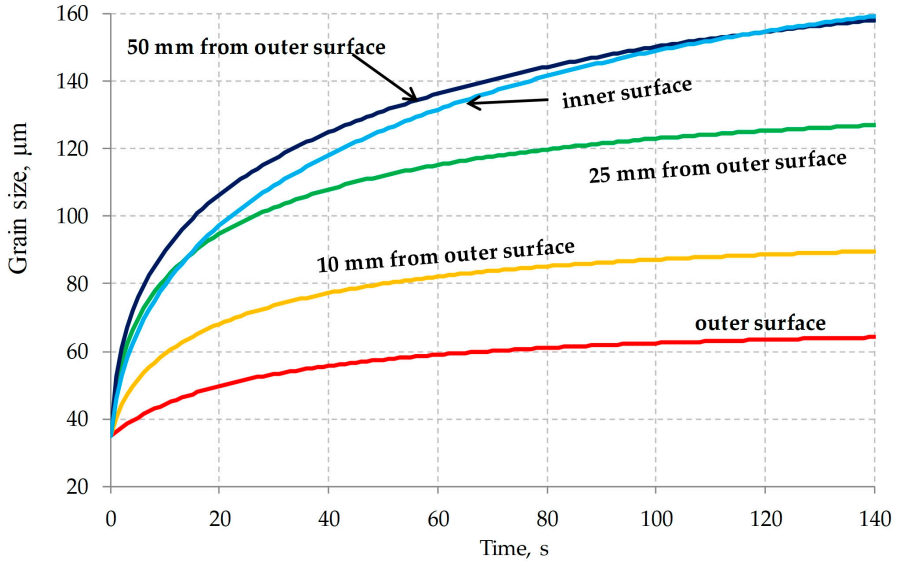


**Figure 12.** Grain growth kinetics at points at different distances from the outer shell surface after elongating.

The calculation results are comparable with the austenitic grains size shown in Figure 1.

## 4. Conclusions

Studies of the growth kinetics of recrystallized austenite grains in AISI 321 stainless steel made it possible to obtain the following results:

1. After holding the steel at a temperature of 1150 °C and above, intensive grain growth is observed. At a temperature of more than 1150 °C and an exposure of more than 5 min, the grain size exceeds a value of 100 μm.
2. Reducing the holding temperature to 1100 degrees leads to a sharp drop in the grain growth rate. The suppression of grain growth is caused by the precipitation of titanium carbides and carbonitrides. The average austenite grain size did not exceed 45 μm even after 15 min exposure at 1100 °C.
3. A dependence is obtained for calculating the kinetics of austenite grain growth for a temperature range of 1150–1250 °C,

$$D^{4.752} - D_0^{4.752} = 1.669 \times 10^{20} \cdot \exp\left(-\frac{359400}{8.314 \cdot T}\right) \cdot t,$$

where $D_0$—initial grain size, μm; $D$—grain size (μm) at the time $t$, (s); $T$—holding temperature, °C.
4. The proposed dependence makes it possible to evaluate grain growth under non-isothermal conditions. To do this, it is necessary to divide the time into small intervals, within which the temperature changes by a small amount (up to 1 °C). The verification of the adequacy of the proposed dependence and the method for calculating the grain size at cooling rates 0.2, 1 and 5 °C/s showed its high convergence. The difference between the calculated and experimental grain size did not exceed 8%.
5. A mathematical model has been developed that combines the solution of the heat conduction equation and the kinetics of grain growth, with the help of which the grain size in the shell after piercing is determined by calculation. The results obtained show that the formation of coarse grains is determined by the kinetics of its post-deformation growth. To obtain a relatively fine-grained microstructure, technological measures should be taken to suppress grain growth.

**Author Contributions:** Conceptualization, A.N.M. and S.V.R.; methodology, A.M.A.; software, D.V.P.; validation, D.V.P., V.N.E. and S.V.R.; formal analysis, A.M.A.; investigation, D.V.P. and S.V.R.; resources, A.N.M., V.N.E. and S.V.R.; data curation, A.M.A. and D.V.P.; writing—original draft preparation, D.V.P.; writing—review and editing, L.V.R.; visualization, L.V.R.; supervision, S.V.R.; project administration, D.V.P. All authors have read and agreed to the published version of the manuscript.

**Funding:** This research received no external funding.

**Data Availability Statement:** Data sharing is not applicable.

**Conflicts of Interest:** The authors declare no conflict of interest.

## References

1. Arroyo, B.; Lacalle, R.; Álvarez, J.A.; Cicero, S.; Moreno-Ventas, X. Analysis of Unexpected Leaks in AISI 316L Stainless Steel Pipes Used for Water Conduction in a Port Area. *Appl. Sci.* **2023**, *13*, 2598. [CrossRef]
2. Resnik, M.; Benčina, M.; Levičnik, E.; Rawat, N.; Iglič, A.; Junkar, I. Strategies for improving antimicrobial properties of stainless steel. *Materials* **2020**, *13*, 2944. [CrossRef] [PubMed]
3. Cadelano, G.; Bortolin, A.; Ferrarini, G.; Bison, P.; Santa, G.D.; Di Sipio, E.; Bernardi, A.; Galgaro, A. Evaluation of the Effect of Anti-Corrosion Coatings on the Thermal Resistance of Ground Heat Exchangers for Shallow Geothermal Applications. *Energies* **2021**, *14*, 2586. [CrossRef]
4. Zhang, F.; O'mahony, J.A.; Miao, S.; Cronin, K. An Experimental Study on the Dilute Phase Pneumatic Conveying of Fat-Filled Milk Powders: Particle Breakage. *Powders* **2023**, *2*, 124–134. [CrossRef]
5. Bykova, A.E.; Sharipzyanova, G.K.; Volgina, N.I.; Khlamkova, S.S. Methodology of Analyzing the Causes of Accidental Failure of Pipes Made of Various Steel Grades. *Russ. Met.* **2018**, *2018*, 1264–1267. [CrossRef]
6. Cheng, J.; Yan, Q.; Pan, Z.; Wei, W. On-Line Measurement and Characterization of Electrochemical Corrosion of 304L Stainless Steel Pipe Wall in High-Speed Cl-Containing Solution. *Metals* **2022**, *12*, 1324. [CrossRef]
7. Zhao, J.; Qiu, F.; Xu, C. Review of Creep-Thermomechanical Fatigue Behavior of Austenitic Stainless Steel. *Crystals* **2023**, *13*, 70. [CrossRef]
8. Kamaya, M. Failure assessment curve for austenitic stainless steel pipes of nuclear power plants. *Eng. Fract. Mech.* **2020**, *238*, 107283. [CrossRef]
9. Vlčková, I.; Jonšta, P.; Jonšta, Z.; Váňová, P.; Kulová, T. Corrosion Fatigue of Austenitic Stainless Steels for Nuclear Power Engineering. *Metals* **2016**, *6*, 319. [CrossRef]
10. Reddy, G.P.; Sandhya, R.; Sankaran, S.; Parameswaran, P.; Laha, K. Creep–fatigue interaction behavior of 316LN austenitic stainless steel with varying nitrogen content. *Mater. Des.* **2015**, *88*, 972–982. [CrossRef]
11. Wang, J.; Su, H.; Chen, K.; Du, D.; Zhang, L.; Shen, Z. Effect of δ-ferrite on the stress corrosion cracking behavior of 321 stainless steel. *Corros. Sci.* **2019**, *158*, 108079. [CrossRef]
12. Kopylov, V.I.; Nokhrin, A.V.; Kozlova, N.A.; Chegurov, M.K.; Gryaznov, M.Y.; Shotin, S.V.; Melekhin, N.V.; Tabachkova, N.Y.; Smetanina, K.E.; Chuvil'deev, V.N. Effect of σ-Phase on the Strength, Stress Relaxation Behavior, and Corrosion Resistance of an Ultrafine-Grained Austenitic Steel AISI 321. *Metals* **2023**, *13*, 45. [CrossRef]
13. Rybalchenko, O.V.; Anisimova, N.Y.; Kiselevsky, M.V.; Belyakov, A.N.; Tokar, A.A.; Terent'ev, V.F.; Prosvirnin, D.V.; Rybalchenko, G.V.; Raab, G.I.; Dobatkin, S.V. The influence of ultrafine-grained structure on the mechanical properties and biocompatibility of austenitic stainless steels. *J. Biomed. Mater. Res. Part B Appl. Biomater.* **2020**, *108*, 1460–1468. [CrossRef] [PubMed]
14. Tiamiyu, A.A.; Eduok, U.; Szpunar, J.A.; Odeshi, A.G. Corrosion behavior of metastable AISI 321 austenitic stainless steel: Investigating the effect of grain size and prior plastic deformation on its degradation pattern in saline media. *Sci. Rep.* **2019**, *9*, 12116. [CrossRef]
15. Seitl, S.; Horník, V.; Lesiuk, G.; Kunz, L. Influence of Micro-structure of selected components made from AISI 304 on the mechanical properties. *Procedia Struct. Integr.* **2023**, *43*, 113–118. [CrossRef]
16. Rezaei, H.; Ghazani, M.S.; Eghbali, B. Effect of post deformation annealing on the microstructure and mechanical properties of cold rolled AISI 321 austenitic stainless steel. *Mater. Sci. Eng. A* **2018**, *736*, 364–374. [CrossRef]
17. Radionova, L.V.; Perevozchikov, D.V.; Makoveckii, A.N.; Eremin, V.N.; Akhmedyanov, A.M.; Rushchits, S.V. Study on the Hot Deformation Behavior of Stainless Steel AISI 321. *Materials* **2022**, *15*, 4057. [CrossRef]
18. Verlinden, B. *Thermo-Mechanical Processing of Metallic Materials*; Verlinden, B., Driver, J., Samaidar, I., Doherty, R.D., Eds.; Elsevier: Amsterdam, The Netherlands, 2007; 528p.
19. Sellars, C.M.; Whiteman, J.A. Recrystallization and grain growth in hot rolling. *Met. Sci.* **1979**, *13*, 187–194. [CrossRef]
20. Harker, D.; Parker, E.R. Grain shape and grain growth. *Trans. Am. Soc. Met.* **1945**, *34*, 156–195.
21. Mats, H. On the theory of normal and abnormal grain growth. *Acta Metallurgica.* **1965**, *13*, 227–238. [CrossRef]
22. Burke, J.E. Some factors affecting the rate of grain growth in metals. *Trans. Am. Iwt. Min. (Metall.) Eng.* **1949**, *180*, 73.
23. Anwar, M.S.; Pradisti, M.G.; Candra, S.A.; Martides, E.; Mabruri, E.; Siradj, E.S. Grain growth kinetics of austenitic stainless steel 316L and the relations between grain sizes and hardness under isothermal conditions. *Metalurgi* **2022**, *37*, 15–20. [CrossRef]

24. Mat, M.F.; Manurung, Y.H.P.; Busari, Y.O.; Adenan, M.S.; Sulaiman, M.S.; Muhammad, N.; Graf, M. Experimental Analysis on Grain Growth Kinetics of SS316L Austenitic Stainless Steel. *J. Mech. Eng.* **2021**, *18*, 97–111. [CrossRef]
25. Annan, K.; Siyasiya, C.; Stumpf, W.; Banks, K.; Tuling, A. Austenite Grain Growth Kinetics in a Low C-Mn Steel and a Ti-Nb-V Microalloyed Steel. *Adv. Mater. Res.* **2014**, *1019*, 327–332. [CrossRef]
26. Manohar, P.A.; Dunne, D.P.; Chandra, T.; Killmore, C.R. Grain Growth Predictions in Microalloyed Steels. *ISIJ Int.* **1996**, *36*, 194–200. [CrossRef]
27. Huda, Z.; Zaharinie, T. Kinetics of grain growth in 2024-T3: An aerospace aluminum alloy. *J. Alloy. Compd.* **2009**, *478*, 128–132. [CrossRef]
28. Huang, Y.-C.; Su, C.-H.; Wu, S.-K.; Lin, C. A Study on the Hall–Petch Relationship and Grain Growth Kinetics in FCC-Structured High/Medium Entropy Alloys. *Entropy* **2019**, *21*, 297. [CrossRef]
29. Alizadeh, R.; Mahmudi, R.; Ngan, A.H.W.; Langdon, T.G. Microstructural stability and grain growth kinetics in an extruded fine-grained Mg–Gd–Y–Zr alloy. *J. Mater. Sci.* **2015**, *50*, 4940–4951. [CrossRef]
30. Rath, B.B.; Lederich, R.J.; Yolton, C.F.; Froes, F.H. Recrystallization and grain growth in metastable beta III titanium alloy. *Met. Trans. A* **1979**, *10*, 1013–1019. [CrossRef]
31. Fei, Y.; Wang, X.N.; Zhu, Z.S.; Li, J.; Shang, G.Q.; Zhu, L.W. β Grain Growth Kinetics of a New Metastable β Titanium Alloy. *Mater. Sci. Forum* **2013**, *747–748*, 844–849. [CrossRef]
32. Mishra, S.; DebRoy, T. Non-isothermal grain growth in metals and alloys. *Mater. Sci. Technol.* **2006**, *22*, 253–278. [CrossRef]
33. Uhm, S.; Moon, J.; Lee, C.; Yoon, J.; Lee, B. Prediction Model for the Austenite Grain Size in the Coarse Grained Heat Affected Zone of Fe-C-Mn Steels: Considering the Effect of Initial Grain Size on Isothermal Growth Behavior. *ISIJ Int.* **2004**, *44*, 1230–1237. [CrossRef]
34. De Sousa, R.C.; Filho, J.C.C.; Tanaka, A.A.; de Oliveira, A.C.S.; Ferreira, W.E.I. Effects of solution heat treatment on grain growth and degree of sensitization of AISI 321 austenitic stainless steel. *J. Mater. Sci.* **2006**, *41*, 2381–2386. [CrossRef]
35. Ghazani, M.S.; Eghbali, B.; Ebrahimi, G. Kinetics and critical conditions for initiation of dynamic recrystallization during hot compression deformation of AISI 321 austenitic stainless steel. *Met. Mater. Int.* **2017**, *23*, 964–973. [CrossRef]
36. Goldstein, M.I. *Special Steels: Textbook for Universities*; Goldstein, M.I., Grachev, S.V., Veksler, Y.G., Eds.; MISiS: Moscow, Russia, 1999; 408p.
37. Mandal, S.; Bhaduri, A.K.; Sarma, V.S. Influence of State of Stress on Dynamic Recrystallization in a Titanium-Modified Austenitic Stainless Steel. *Met. Mater. Trans. A* **2012**, *43*, 410–414. [CrossRef]
38. Kratochvíl, P.; Lukáč, P.; Vostrý, P.; Pacák, J.; Tomeš, J. Dynamic softening and static recrystallisation of AISI 321 steel. *Mater. Sci. Technol.* **1991**, *7*, 78–82. [CrossRef]
39. Perevozchikov, D.V. *Improvement of Manufacturing Technology Hot-Rolled Pipe from Steel Grade 08KH18N10T to Improve the Structure 2.6.4—Metal Forming: Dissertation Degree of Candidate of Technical Sciences*; Danil Viktorovich Perevozchikov: Chelyabinsk, Russia, 2022; 161p.
40. Solodov, A.P. *Heat and Mass Transfer in Power Plants. Engineering Methods of Calculation. Electronic Resource [Text]: Textbook on the Courses "Heat and Mass Transfer in NPP Equipment" for Students Studying in the Areas of "Nuclear Energy and Thermal Physics" and "Heat Power Engineering and Heat Engineering"/A.P. Solodov*; MEI Publishing House: Moscow, Russia, 2015; 124p, ISBN 978-5-046-1636-8.
41. Available online: http://jmatpro.ru/ (accessed on 31 May 2023).
42. Samarsky, A.A. *Computational Heat Transfer*; Samarsky, A.A., Vabishchevich, P.N., Eds.; Editorial URSS: Moscow, Russia, 2003; 784p.
43. Kuznetsov, G.V. *Difference Methods for Solving Problems of Heat Conduction*; Kuznetsov, G.V., Sheremet, M.A., Eds.; Publishing House of the Tomsk Polytechnic University: Tomsk, Russia, 2007; 172p.
44. Rushchits, S.V.; Akhmed'yanov, A.M.; Perevozchikov, D.V.; Makovetskiy, A.N.; Eremin, V.N. Modelling of Hot Deformation of Steel 08H18N10T (AISI 321) under Uniaxial Compression Test. *Bull. South Ural. State University. Ser. Metall.* **2021**, *21*, 30–41. (In Russian)
45. Eremin, V.N.; Perevozchikov, D.V.; Makovetskiy, A.N.; Shakirova, L.I.; Rushchits, S.V. Formation of the Structure of Steel 08KH18N10T during Pilgrim Rolling and Following Annealing. *Bull. South Ural. State University. Ser. Metall.* **2021**, *21*, 78–86. (In Russian) [CrossRef]